Manganese and tyrosyl radical function in photosynthetic oxygen evolution

Cecilia Tommos*†, Curtis W Hoganson*, Marilena Di Valentin*, Nikos Lydakis-Simantiris*‡, Pierre Dorlet*§, Kristi Westphal*, Hsiu-An Chu*, John McCracken* and Gerald T Babcock*

Photosystem II catalyzes the photosynthetic oxidation of water to O_2. The structural and functional basis for this remarkable process is emerging. The catalytic site contains a tetramanganese cluster, calcium, chloride and a redox-active tyrosine organized so as to promote electroneutral hydrogen atom abstraction from manganese-bound substrate water by the tyrosyl radical. Recent work is assessed within the framework of this model for the water oxidizing process.

Addresses
*Department of Chemistry, Michigan State University, East Lansing, MI 48824, USA
†The Johnson Research Foundation, Department of Biochemistry and Biophysics, University of Pennsylvania, Philadelphia, PA 19104, USA
‡Division of Biological Sciences, The University of Michigan, Ann Arbor, MI 48109-1048, USA
§Section de Bioénergétique, Département de Biologie Cellulaire et Moléculaire, CEA Saclay, 91191 Gif-sur-Yvette, Cedex, France
Correspondence: Gerald T Babcock
e-mail: babcock@cemvax.cem.msu.edu

Current Opinion in Chemical Biology 1998, 2:244–252

http://biomednet.com/elecref/1367593100200244

Abbreviations

BDEs	bond dissociation energies
OEC	oxygen-evolving complex
PSII	photosystem II

Introduction

Plant and algae use water as the ultimate electron donor to the photochemical pathway that occurs in Photosystem II (PSII). Reducing equivalents that are eventually used for CO_2 fixation are generated in this process, and O_2 is released as the product of the water oxidation chemistry. PSII occurs as a multi-polypeptide complex in the thylakoid membranes of chloroplasts and contains a variety of cofactors essential to the photochemical and redox processes it catalyzes (for recent reviews see [1••,2,3,4••,5••,6•,7••]). A chlorophyll complex, designated P680, and a bound quinone, Q_A, lie at the heart of the photochemistry, as the initial light-driven event generates the $P680^+Q_A^-$ state. Regeneration of the photoactive $P680Q_A$ state oxidizes H_2O to O_2 and requires the participation of four manganese ions, calcium, chloride and a redox-active tyrosine, Y_Z, which has been identified as Tyr161 on the D1 protein [2]. These reactions are summarized in Figure 1. Recent data indicate that the metal–tyrosine center functions as an integral unit and forms the catalytic site in PSII, denoted the oxygen-evolving complex (OEC) [8–10,11••]. The coupling of the one-electron photochemistry at $P680Q_A$ to the four-electron $2H_2O \rightarrow O_2 + 4H^+ + 4e^-$ chemistry at the OEC, occurs independently in each of the PSII enzymes and produces striking period four oscillations in O_2 production under single turnover conditions [1••]. The $(Mn)_4$ cluster accumulates oxidizing equivalents linearly with photons absorbed; the status of the cluster on its course to water oxidation is designated by the S_n notation, where the subscript denotes the number of stored oxidizing equivalents. Only after formation of S_4 does water oxidiation proceed.

Figure 1

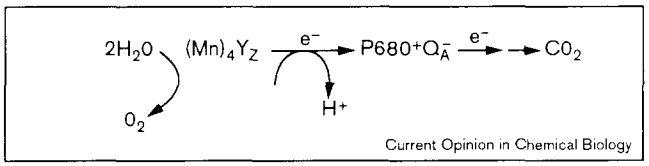

An overview of the electron transfer chemistry following the light absorption and photochemical processes that produce the charge separated state, $P680^+Q_A^-$, in PSII. The Q_A species is regenerated by further electron transfers that eventually deliver the electron on Q_A to CO_2. P680 is restored by electron transfer from water, which ultimately produces O_2 through the $(Mn)_4Y_Z$ complex.

Data on the physical structure of the $(Mn)_4Y_Z$ site, on its ligation into PSII and on Mn valences has come from a variety of sources [1••,5••,12]. These have been summarized recently to provide a model for the catalytic site in the S_0 state that places Y_Z at the open end of a C-shaped tetranuclear $(Mn)_4$ cluster and hydrogen-bonded to His190 on the D1 protein (D1–His190; Figure 2; [7••,13,14••]; see also [15]. The two non redox-active cofactors, Ca^{2+} and Cl^-, that are required for O_2 evolution are also likely to be part of the active site [5••,12,16]. Substrate water ligates to the two manganese ions at the open end of the C-shape and hydrogen bond to the tyrosyl oxygen. Production of the neutral $Y_Z^•$ radical involves electron transfer to $P680^+$ generated by the photochemical reactions and concurrent deprotonation through the His190. The proton makes its way through the protein matrix and is eventually released to the thylakoid lumen. The structure of the $(Mn)_4Y_Z^•$ site provides an ideal geometry for the hydrogen atom abstraction

chemistry that is characteristic of radical function in the general class of metalloradical enzymes and leads to a complete model for the S-state cycle (Figure 3) [7••]. The general principles of the reaction scheme are described in Figure 3. This model provides an overall hypothesis for water oxidation that can be examined within the context of recent experimental work. This commentary focuses on reviewing these developments and on assessing recent results within the context of this model.

Figure 2

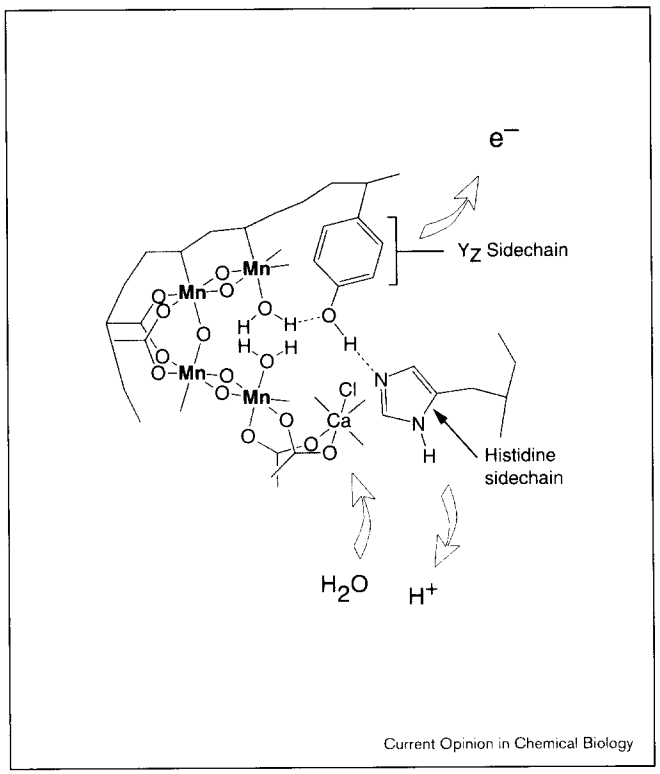

Postulated structure for the Photosystem II water-oxidizing site in its S_0 state. The substrate-binding metal cluster is closely associated with the redox-active Y_Z tyrosine, which is hydrogen bonded to substrate water and to D1–His190. The arrows demonstrate the flow of water, electrons and protons through the catalytic site that we envision.

Thermodynamics and structure in the S-state cycle

The individual S-state transitions are only weakly driven; the higher equilibrium constant for the $S_0 \rightarrow S_1$ transition reflects the fact that S_1 is the dark-stable state of the system (Table 1) [17]. For radical-based atom-abstraction processes, entropic contributions to the overall driving force are usually close to zero and, thus, bond-dissociation energies (BDEs) become useful predictors of overall reaction spontaneity [18,19]. The high BDEs for water and hydroxide ion were early sources of concern as the BDE for the tyrosine O–H bond is ~87 kcal/mol [20]. Thus, the reaction that occurs on $S_0 \rightarrow S_1$, which can be viewed superficially as

$$\begin{array}{l} H_2O \rightarrow OH^{\bullet} + H^{\bullet} \\ H^{\bullet} + Y_ZO^{\bullet} \rightarrow Y_ZOH \\ \hline H_2O + Y_ZO^{\bullet} \rightarrow OH^{\bullet} + Y_ZOH \end{array} \quad \begin{array}{l} \Delta H = 119\ \text{kcal/mol} \\ \Delta H = -87\ \text{kcal/mol} \\ \hline \Delta H = +32\ \text{kcal/mol} \approx \Delta G \end{array} \quad (1)$$

appears to be significantly unfavorable. Recent theoretical and experimental work has allayed these concerns by showing that water ligation to Mn lowers the BDEs for water and hydroxide dramatically [21••,22,23,24••]. Figure 4 summarizes the computational results, which correctly predicted the experimental data by showing that the BDE for the O–H bond in water decreases by ~35 kcal/mol, when bound terminally to Mn(III) in an Mn_2O_2 diamond-shape structure. The calculations show a similar decrease for the hydroxide O–H bond when ligated to a binuclear Mn cluster.

These experimental and computational thermodynamic data rationalize a mechanistic puzzle in forming oxygen from water in PSII. That is, the one-electron potentials for oxidizing water vary widely and must be leveled in the OEC so that the relatively constant one volt $Y_Z^{\bullet}$ oxidant can effectively advance each S-state transition [7••]. As Figure 4 shows, this is done by hydrogen abstraction from H_2O and OH^- ligated to the Mn cluster, as the BDEs for these two substrates are essentially identical and only slightly weaker than that of the tyrosyl O–H bond, as the equilibrium constants for the individual $S_nY_Z^{\bullet} \leftrightarrow S_{n+1}Y_Z$ steps indicate. Moreover, the overall electroneutral S-state advance, postulated for each transition in Figure 3, avoids uncompensated charge buildup in the OEC as it proceeds through the cycle. Practically, this aspect of the mechanism means that electrostatic penalties involved with burying charge in a region of low dielectric will not be encountered. As the driving force available in PSII for the S-state transitions is quite low, maintaining electroneutrality is critical to the thermodynamic feasibility of water oxidation.

The BDE results also provide insight into one of the key questions associated with water oxidation, that is, whether substrate water molecules ligate as terminal or bridging ligands in the OEC as illustrated in Figure 5. The equilibrium constants noted above suggest that each step of the S cycle occurs under almost thermoneutral conditions, that is, that the difference in BDE between substrate and the Y_Z–OH bond is small. Pecoraro and co-workers [23,24••] have addressed this issue directly by measuring BDEs for both terminal and bridging aqueous ligands. For six terminal complexes, the average BDE was 87 kcal/mol; for four bridging O–H bonds, the average BDE was 79 kcal/mol, significantly lower than that of the tyrosyl O–H at 87 kcal/mol. This comparison reinforces our suggestion that substrate water binds terminally to the Mn_2O_2 diamonds, if the hydrogen atom abstraction model

Figure 3

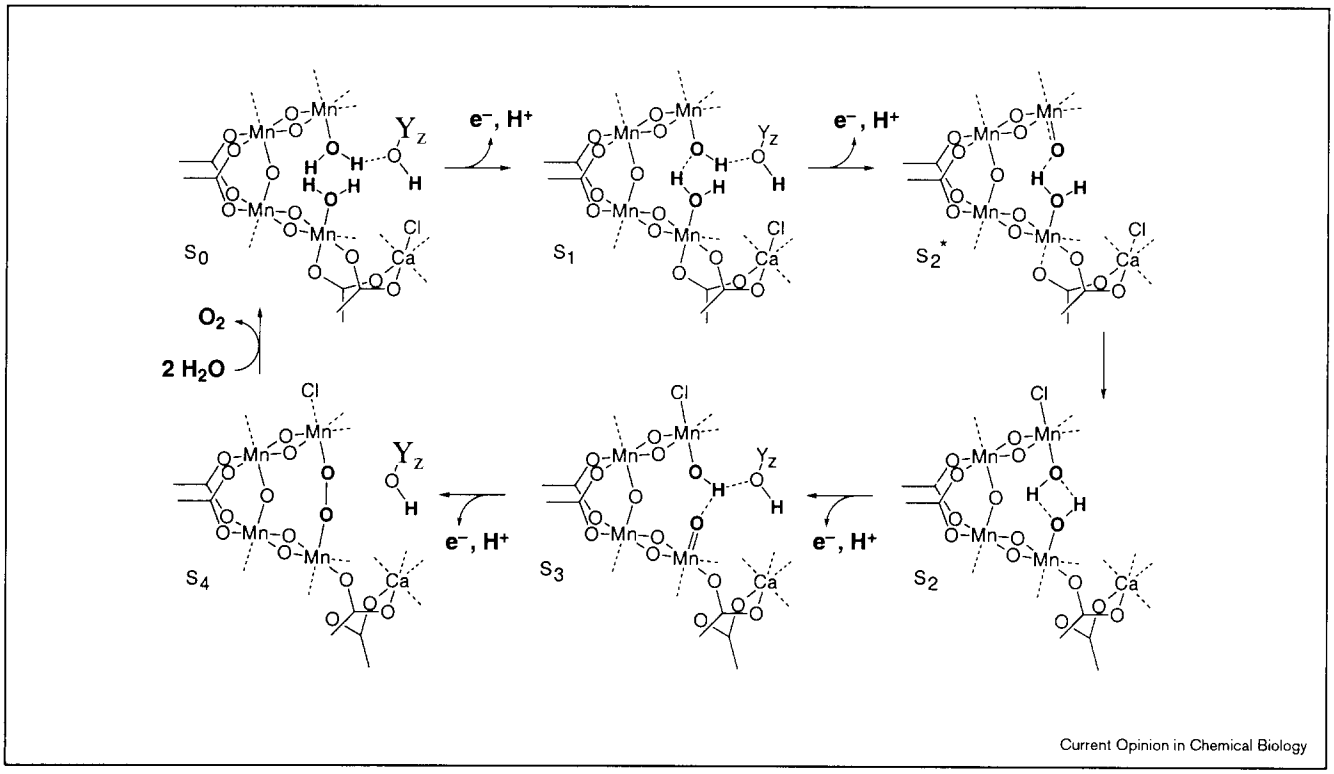

The proposed reaction sequence for the water-splitting chemistry catalyzed by Photosystem II. The initial transition from $S_0 \rightarrow S_1$ illustrates the general operational principal. Upon reduction of $Y_Z^{\bullet}$, hydrogen abstraction from the substrate water to which it is hydrogen bonded occurs. The oxidizing equivalent generated in the process delocalizes to the $(Mn)_4$ cluster to increase its oxidation state by one. Repeated application of this scenario through the remaining S-state transitions eventually strips the four hydrogens from the substrate water molecules and sets up conditions for the formation of the oxygen–oxygen bond. This occurs via a concerted process in the $S_3 \rightarrow S_4 \rightarrow S_0$ transition [14••]. The S_2^* state occurs as a transient intermediate that rearranges to the more stable S_2 state.

in Figures 2 and 3 is fundamentally correct for the water oxidation process.

Kinetics of the S-state advances and relationship to the structure of the active site

Despite the small driving forces for the S-state transitions, they proceed rapidly and with remarkably low activation energies (Table 1). Both of these kinetics aspects of the operation of the OEC are well accommodated in the hydrogen-transfer processes envisioned in Figure 3. Early physical organic chemistry work shows that radical-mediated hydrogen abstraction from an O–H bond, as opposed to abstraction from a C–H bond, proceeds surprisingly quickly, even at very low driving forces [18]. Moreover, the low activation energies suggest that the reaction coordinate for the atom-abstraction process has substantial concerted character.

The postulated atom-transfer characteristics of the S-state advances have been examined recently by three groups, who have each carried out hydrogen/deuterium (H/D) kinetic-effect measurements on PSII (Table 1) [25–27]. The results are consistent in showing that moderate isotope effects on the rates of the reaction occur, although there are some differences in detail. Surprisingly, the measured isotope effects are quite sensitive to the specifics of sample preparation. This observation correlates well with the fact that the rates of the S-state transitions themselves depend on the manner in which the sample is prepared, on the binding status of three extrinsic subunits that are closely associated with PSII on the lumenal side of the membrane, and on the extent to which the Ca^{2+} and Cl^- cofactors have been perturbed or substituted. Sr^{2+}, for example, will substitute for Ca^{2+}, but supports only ~40% of the native O_2-evolution activity and produces a reduction in the rates of the four S-state transitions [28] (K Westphal, GT Babcock, unpublished data). Similarly, Pace and co-workers [29,30•] have shown that the S-state cycle is slowed on all transitions in PSII-membrane preparations, as compared to more native thylakoid samples. The strong dependence of the rates of S-state advance on sample conditions suggests that small perturbations in structure have kinetically significant consequences. Hydrogen atom transfers, because of the large mass of the proton relative to the electron, have very short tunneling distances (that is, the distance over which a particle can penetrate a barrier) and are expected to be much more sensitive to structure than

Table 1

Characteristics of the S-state transitions in Photosystem II.

Characteristic	Thylakoids	PSII membranes	PSII core particles	References
Half-times for S-state advance				
$S_0 \rightarrow S_1$	40–60 μs	30–70 μs	60 μs	[2,25,26,29,30•]
$S_1 \rightarrow S_2$	65–85 μs	55–110 μs	75–95 μs	
$S_2 \rightarrow S_3$	140–245 μs	180–350 μs	225–380 μs	
$S_3 \rightarrow S_4 \rightarrow S_0$	750 μs; 1.3 ms	1.2–1.4 ms	4.1–4.6 ms	
Activation energies (kJ/mol)				
$S_0 \rightarrow S_1$		5.0		
$S_1 \rightarrow S_2$		12.0	14.6–14.8	[25,26]
$S_2 \rightarrow S_3$		36.0	35.0	
$S_3 \rightarrow S_4 \rightarrow S_0$		20.0/46.0	21.0/67.0; 37.5	
Kinetic isotope effects (k_H/k_D)				
$S_0 \rightarrow S_1$			1.3	[25–27]
$S_1 \rightarrow S_2$	1.2	1.3; 2.9	1.3–1.6	
$S_2 \rightarrow S_3$	2.4	1.3	2.1–2.3	
$S_3 \rightarrow S_4 \rightarrow S_0$	1.4	1.4–1.6	1.4–1.5	
Equilibrium constants				
$S_0 \rightarrow S_1$		$\geq 10^5$		[17]
$S_1 \rightarrow S_2$		$\sim 10^1$		
$S_2 \rightarrow S_3$		$\sim 10^1$		
$S_3 \rightarrow S_4 \rightarrow S_0$*		$\sim 10^1$		

*The $S_3 \rightarrow S_4 \rightarrow S_0$ value is an estimation based on the reduction potentials of the three lower S-state transitions and Y_Z, and the potential required for water oxidation.

is a pure electron-transfer process [31]. This suggests that the sensitivity of PSII kinetic phenomena to sample conditions reflects the involvement of atom transfer in the reaction coordinate for the S-state cycle, consistent with the notion that atom abstraction is fundamental to catalysis.

The exquisite sensitivity of the rate of an atom transfer reaction to the geometric arrangement of the donor/acceptor pair has important consequences for the structure of the $(Mn)_4Y_Z$ site. Several groups have used magnetic resonance methods to estimate the distance between $Y_Z^\bullet$ and the metal cluster. Fundamental to this effort is the fact that perturbations to the Ca^{2+} or Cl^- cofactors inhibit water splitting. With this inhibition in effect, the OEC can be trapped in a state in which the electron paramagnetic resonance (EPR) spectrum from $Y_Z^\bullet$ is split ($\Delta H \approx 90$–240 Gauss) by a magnetic interaction with the manganese S_2 state. Rutherford and co-workers [32] were the first to discover this magnetic interaction and the split EPR signal; Nugent and co-workers [33], initially, and Britt and his co-workers [10,11••], conclusively, demonstrated its $S_2Y_Z^\bullet$ origin.

The splitting in the spectrum suggests dipolar (D) and/or exchange (J) interaction between $(Mn)_4$ and $Y_Z^\bullet$. Boussac *et al.* [32] used spectral simulation to estimate a value for J and suggested that dipole–dipole interactions produced line broadening in the spectrum. MacLachlan *et al.* [34] studied the $S_2Y_Z^\bullet$ spectrum in samples in which both Ca^{2+} and Cl^- binding were perturbed by acetate addition and invoked a dominant J coupling; their simulations provided a separation of 9 Å between $Y_Z^\bullet$ and the metal cluster. More recently, Britt's group [15] has reinvestigated the $S_2Y_Z^\bullet$ spectrum in acetate-treated PSII. Under these conditions, the $S_2Y_Z^\bullet$ lineshape is suggestive of a Pake pattern and pure dipolar coupling. With this assumption, a distance of 3.5 Å was obtained by simulation. Brudvig and collaborators explored the spectrum in acetate-inhibited samples and concluded that substantial J coupling had to occur, in addition to the dipolar coupling favored by Britt and co-workers (GW Brudvig, personal communication). Their distance estimate relied on a distributed dipole analysis, originally developed by Khangulov *et al.* [35], and fell in the 6–10 Å range. In work we have carried out recently, spectral simulation was used to conclude that both J and D contributions are necessary to reproduce the $S_2Y_Z^\bullet$ lineshape in acetate-treated or Ca^{2+}-depleted preparations and to determine an upper limit of the $(Mn)_4$–$Y_Z^\bullet$ distance as ~8 Å (P Dorlet, M Di Valentin, GT Babcock, J McCracken, unpublished data). In the calculations described above, the distance is defined as that between the center of the tyrosyl aromatic ring and the effective magnetic center of the $(Mn)_4$ cluster. Overall, these distance estimates rely on discriminating between the J and D coupling contributions to the observed splittings. Literature precedent favors a substantial J coupling at distances less than 9–10 Å [36]. If this is the case in PSII, and we regard this as likely, then the longer, distance (~8 Å) is the more appropriate. Such a distance is consistent with the structure for the $(Mn)_4Y_Z$ cluster shown in Figure 2.

Figure 4

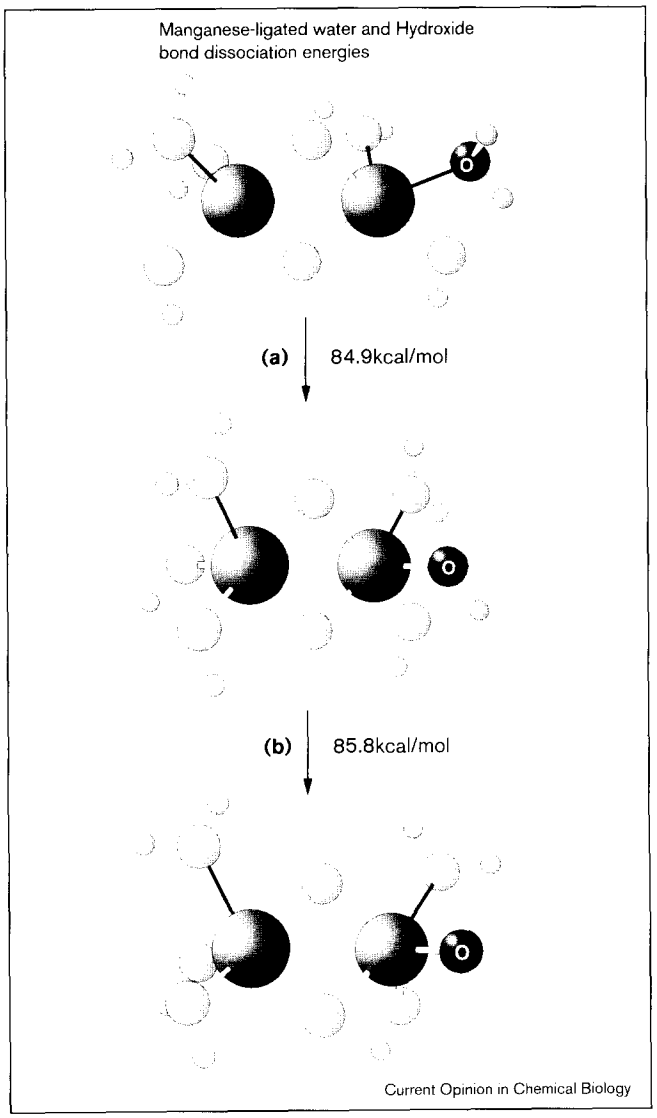

Calculated O–H bond dissociation energies (BDEs) for manganese-ligated water and hydroxide. The derived BDEs are **(a)** 84.9 kcal/mol for water and **(b)** 85.8 kcal/mol for hydroxide [21••].

In addition to being in the direct vicinity of the $(Mn)_4$ cluster, Y_Z is predicted to be involved in a bifurcated hydrogen bond at several points in the proposed reaction sequence for the OEC. This prediction has been tested recently by pulsed EPR applied on the $S_2Y_Z^{\bullet}$ signal in acetate-treated [15] and Ca^{2+}-depleted (C Tommos, J McCracken, S Styring, GT Babcock, unpublished data) PSII. These two studies provide evidence that $Y_Z^{\bullet}$ is involved in two hydrogen bonds to isotope-exchangeable protons, consistent with the proposed mechanism. The hydrogen-bonding status is dramatically changed and a similar bifurcated interaction is not observed in samples devoid of the $(Mn)_4$ cluster [2,8].

Figure 5

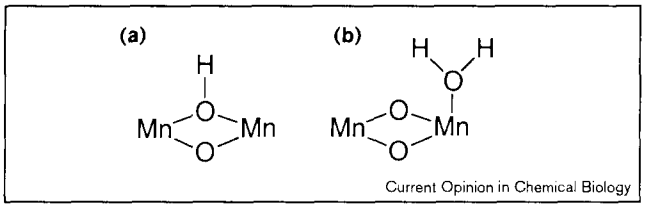

Possible modes of substrate water ligation in a Mn_2O_2 diamond structure. In **(a)** a bridging ligand is viewed as providing the abstractable hydrogen and the oxygen substrate is eventually released as O_2. In **(b)**, the substrate binds at the terminal position on the Mn_2O_2 core.

The $(Mn)_4$—$Y_Z^{\bullet}$ distance estimates that have been made thus far involved samples that have impaired O_2 evolution. Recent Fourier transform infrared (FTIR) work, however, indicates that the close radical/metal-cluster proximity that has been inferred will persist to the functional system [37••]. These results, together with the initial observations of EPR signals from the S_0 state [38•,39•], hold promise for generating a more precise understanding of the geometry of the $(Mn)_4Y_Z$ site in the water-splitting center.

Proton currents and the implications for water oxidation

An essential feature of the postulated mechanism in Figure 3 is that Y_Z sloughs its proton upon each of its redox cycles so that the neutral radical is available for hydrogen atom abstraction from Mn-ligated substrate. This requirement is shown explicitly in Figure 2, where Y_Z serves in a H atom 'divider' capacity. By abstracting substrate hydrogens, Y_Z maintains both an electron current to the photo-oxidized $P680^+$ species and a proton current to the thylakoid lumen through the catalytically essential D1–His190. Additional amino acids most probably function with His190 to provide an effective proton efflux channel, analogous to those that occur in the terminal respiratory enzyme, cytochrome oxidase, and in the bacterial reaction center [40,41]. This model predicts that proton release should occur stoichiometrically with each of the S-state transitions and that the release should be initiated by the Y_Z oxidation. The model makes the further prediction that the $(Mn)_4Y_Z$ site should maintain overall electroneutrality as it proceeds through the catalytic cycle. Two experimental methods, proton-release measurements and optical detection of chromophore bandshifts upon redox transition at Y_Z and $(Mn)_4$, are relevant to these issues and have been applied to PSII (for reviews, see [4••,42]). The results from this work can be used to test these predictions.

Proton release

A proton release pattern of 1:1:1:1 accompanies the four S-state transitions in PSII core preparations, as predicted by Figures 2 and 3 [42]. Moreover, the kinetics of the

proton release are rapid. These two sets of observations provide strong support for the hydrogen atom abstraction model. In membrane-containing samples, however, the release pattern becomes more complex and is dependent on both the details of the preparation and on pH [42]. In PSII membranes, for example, the $S_0 \rightarrow S_1$ transition is accompanied by 1–1.75 H^+ released; the higher number is observed at lower pH and declines to 1 with a pK_a of ~6.2 as the pH is increased. The proton flux on $S_0 \rightarrow S_1$ appears to correlate inversely with the $S_3 \rightarrow S_4 \rightarrow S_0$ release. These observations suggest that the water-splitting system resets itself in a pH-dependent manner, which may reflect acid-base effects in the proton-transfer pathway associated with $Y_Z^{\bullet}$. Recent measurements on samples in which the $(Mn)_4$ cluster has been removed reinforce this conclusion, as proton release upon Y_Z oxidation is also pH dependent and modulated by a group with $pK_a \sim 6$ [43•,44••]. The alternative interpretation of the compensating releases on $S_0 \rightarrow S_1$ and $S_3 \rightarrow S_4 \rightarrow S_0$, that is, that substrate loads as molecular water at low pH and as hydroxide at higher pH, is disfavored by model compound results from Pecoraro and his colleagues that show that the pK_a of Mn-bound water is quite high [23,24••], if the overall charge on the cluster is low, as we postulate. Proton release during the $S_1 \rightarrow S_2$ transition in PSII membranes is also pH dependent, varying from 0–0.5 across the physiological pH range [42]. The pH profile shows clear evidence of an electrostatic shift in pK_a, from 8.2 in S_1 to 7.25 in S_2, which suggests either charge accumulation or internal charge rearrangement in the OEC on this S-state transition. We have argued elsewhere [7••] in favor of charge rearrangement in the cluster as the likely basis for the S-state-dependent pK_a shift and used it, in addition to other arguments, to suggest the Cl^- motion during $S_1 \rightarrow S_2$ in Figure 3. Mechanistically, Cl^- migration from Ca^{2+} to $(Mn)_4$ on this transition is regarded as essential in maintaining contact between $Y_Z^{\bullet}$ and abstractable substrate hydrogens in the higher S-states.

Figure 6

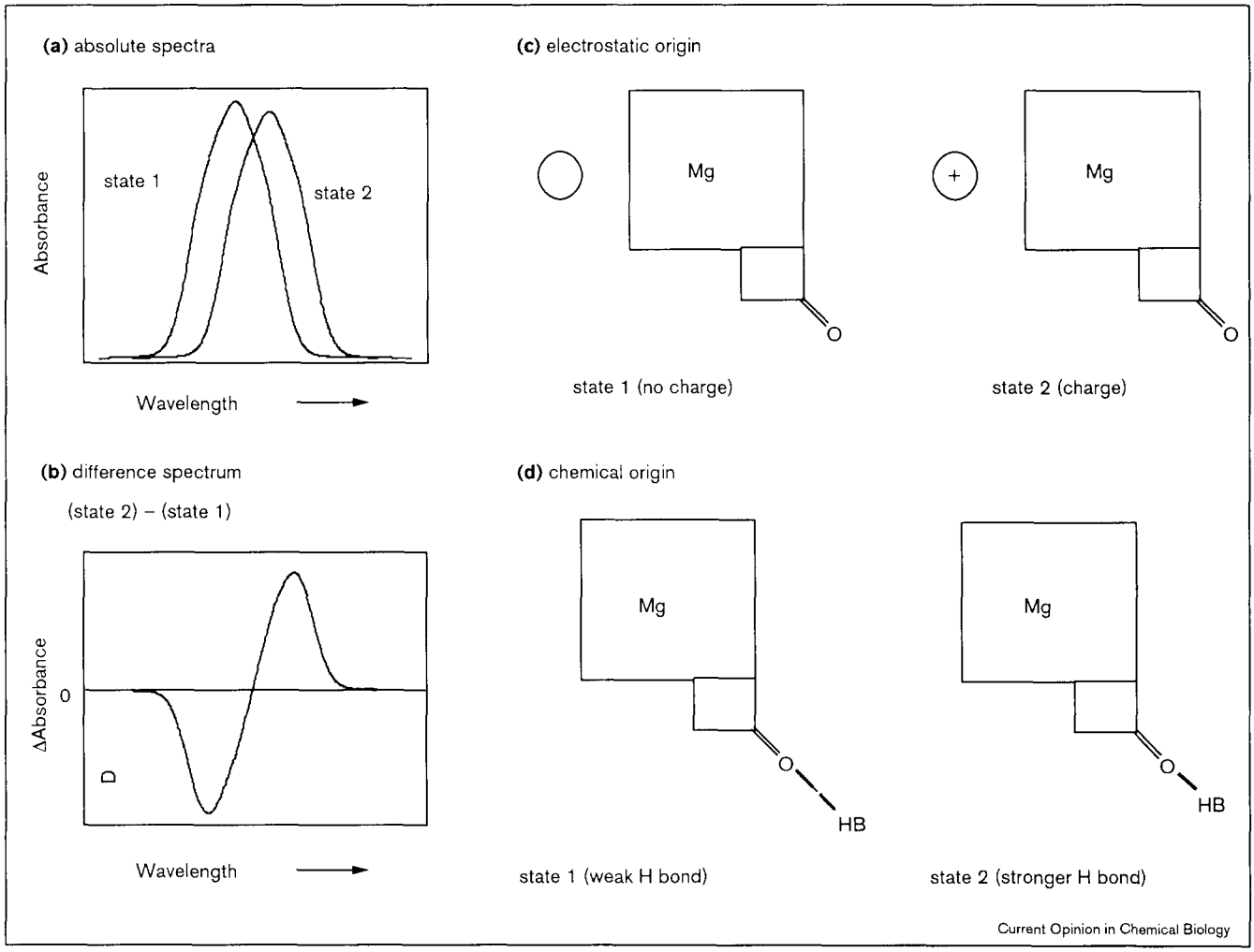

Physical basis for chromophore absorption bandshifts. **(a)** Absolute spectra. **(b)** Difference spectra. **(c)** Electrostatic origin. **(d)** Chemical origin. (See text for full details).

Chlorophyll bandshifts

Phenomena associated with chromophore bandshifts are more subtle than those associated with proton release and the rationale that underlies their application and interpretation is summarized, conceptually, in Figure 6. In Figure 6a, the absolute absorption spectra of a chromophore in two different states of the system, for example, in the Y_Z and $Y_Z^\bullet$ states or in the S_1 and S_2 states, are shown. The assumption is made that the interaction of the chromophore with its environment is dependent on the state of the enzyme so that a shift to longer wavelength (a redshift) occurs in state 2, relative to state 1. The (state 2)–(state 1) difference spectrum (Figure 6b) shows this absorption redshift as a derivative-shaped feature, negative to short wavelength, positive to longer wavelength, for this specific example. These kinds of bandshifts have been measured extensively in photosynthetic systems and are usually interpreted as reflecting electrostatic events. This is shown schematically in Figure 6c, where the responding pigment is taken as being a chlorophyll. In state 1, there are no charges in its environment; upon the state 1→state 2 transition, a charge is generated that alters the absorption and produces the bandshift shown in Figure 6a,b. Under these conditions, the chromophore bandshift is referred to as 'electrochromic' and provides a probe of charge creation, movement, and rearrangement in photosynthetic systems. Alternatively, chromophore bandshifts can have a chemical origin, as shown in Figure 6d. In this example, state 1 represents a chlorophyll having a weak hydrogen bond to its 9-keto C=O group; in state 2, this hydrogen bond strengthens, which will produce Q_y and Soret absorption redshifts [45] and generate the spectrum shown in Figure 6b. The 'Q_y' and 'Soret' notation refer to specific regions of the optical absorption spectrum of chlorophyll species. The Q_y band is in the red region of the spectrum and the Soret is in the blue.

With this background, we are in a position to interpret the optical bandshifts that have been observed during the water-splitting process within the context of Figure 3. Two different classes of bandshifts have been observed. In the first, the chlorophyll absorption change persists throughout the lifetime of the S state. These bandshifts have been observed for the $S_1 \rightarrow S_2$ transition and are reversed upon $S_3 \rightarrow S_4 \rightarrow S_0$ [4••]. In the Q_y region, the shape of the bandshift in the S_2–S_1 spectrum is an increase to the blue (to a shorter wavelength) and a decrease to the red [46], whereas, in the Soret, the phase of the shift is reversed [4••]. The stable S_2–S_1 bandshifts in the visible and the Soret spectral regions correlate well with the pK_a shift noted above for proton release during the $S_1 \rightarrow S_2$ transition and reinforce the likelihood that both proton release and the chlorophyll spectrum respond to the Cl^- charge movement envisioned in Figure 3. The persistent $S_1 \rightarrow S_2$ bandshift can be interpreted as reflecting a modified version of the electrostatically induced events in Figure 6c, in which the PSII pigments respond to a charge rearrangement within the OEC, rather than to charge accumulation.

The second class of pigment bandshift that has been observed in PSII has been studied extensively recently and accompanies the Y_Z redox cycle [43•,44••,47]. In contrast to the persistent bandshifts discussed above, these absorption changes are transient and rise and decay on the microsecond and millisecond timescale. The groups that have studied the transient bandshifts interpret them in terms of retained positive charge at $Y_Z^\bullet$, which is clearly counter to the predictions of Figures 2 and 3. Junge and co-workers [44••], in particular, have argued that these observations invalidate a hydrogen atom abstraction function for $Y_Z^\bullet$. Several points, however, argue against this interpretation. First, if a charge at the $Y_Z^\bullet$ site electrostatically induces H^+ release, one may expect that the pigment bandshift would respond to the resulting electrostatic relaxation in the protein. The decay of the transient bandshifts, however, does not correlate with the H^+ release that occurs during the lifetime of $Y_Z^\bullet$ [43•]. Second, the proposal that uncompensated positive charge is retained at $Y_Z^\bullet$ to induce proton release electrostatically is undermined by recent data that indicate that the $Y_Z^\bullet$ site is readily accessible to the surrounding aqueous medium (RJ Debus, personal communication; C Tommos, J McCracken, S Styring, GT Babcock, unpublished data). Debus's results showing that exogenous imidazole can restore Y_Z oxidation in D1–His190 mutants sets the timescale of this accessibility in the submillisecond regime. This accessibility and the high energetic cost of burying uncompensated charge in regions of low dielectric considerably diminish the likelihood of a charged $Y_Z^\bullet$ site. Finally, the shape of the transient pigment bandshifts differs dramatically from those discussed above for the persistent $S_1 \rightarrow S_2$ optical changes. In the chlorophyll Q_y region, the sense of the $Y_Z^\bullet$–Y_Z change is opposite in sign to that of the S_2–S_1 change [46], whereas the two show the same overall shape in the Soret [4••]. Thus, the transient bandshift corresponds to absorbance redshifts in both the visible and the Soret region, whereas the persistent bandshift is to the red in the Soret but to the blue in the visible. Given this sign difference and the fact that Y_Z and the $(Mn)_4$ cluster are spatially close, it is unlikely that both the $Y_Z^\bullet$–Y_Z and S_2–S_1 bandshifts are of electrostatic origin. The weight of the evidence favors a true electrochromic origin for the persistent bandshifts, as noted above, which suggests that an explanation other than electrostatic must be sought for the transient response.

Data to support a chemical origin for the transient chlorophyll bandshifts have emerged recently. The changes in hydrogen bond strength shown schematically in Figure 6d should be manifest in two ways: the optical absorption spectrum in both the Soret and visible regions should redshift as the hydrogen bond strengthens [45] and the vibrational frequency of the keto C=O stretching

vibration should decrease as this occurs. The absorption redshifts have been discussed above, and recent FTIR data from Wydrzynski and co-workers [48•] show that there is a corresponding decrease in a vibrational mode in the 1700 cm^{-1} region that can be assigned to a chlorophyll keto group as $Y_Z^{\bullet}$ is formed. Taken together, the inconsistencies in attributing the transient pigment shifts in the $Y_Z^{\bullet}$–Y_Z spectrum to an electrostatic origin and the positive evidence above linking redox reactions at Y_Z to changes in hydrogen-bond strength at a chlorophyll keto group indicate that a retained charge at the $Y_Z^{\bullet}$ site is highly unlikely. The coupling between Y_Z redox state and chlorophyll hydrogen bonding may have important implications for PSII function, but this possibility remains to be explored.

Acknowledgements

The work performed at Michigan State University that is included in this article was supported by the Human Research Frontiers Program, the United States Department of Agriculture National Research Initiative Competitive Grants Program and the National Institutes of Health.

References and recommended reading

Papers of particular interest, published within the annual period of review, have been highlighted as:

- • of special interest
- •• of outstanding interest

1. •• Britt RD: **Oxygen evolution.** In *Oxygenic Photosynthesis: The Light Reactions.* Edited by Ort DR, Yocum CF. Dordrecht: Kluwer Academic Publishers; 1996:137-164.
Britt reviews the status of magnetic resonance studies of the $(Mn)_4$ cluster with both conventional and double resonance techniques and presents a critical evaluation of current models for the mechanism of water oxidation.

2. Diner BA, Babcock GT: **Structure, dynamics, and energy conversion efficiency in photosystem II.** In *Oxygenic Photosynthesis: The Light Reactions.* Edited by Ort DR, Yocum CF. Dordrecht: Kluwer Academic Publishers; 1996:213-247.

3. Nugent JHA: **Oxygenic photosynthesis: electron transfer in photosystem I and photosystem II.** *Eur J Biochem* 1996, **237**:519-531.

4. •• Witt HT: **Primary reactions of oxygenic photosynthesis.** *Ber Bunsenges Phys Chem* 1996, **100**:1923-1942.
Time-resolved optical methods have been invaluable in providing kinetic, thermodynamic, and electrostatic insight into photosynthetic water oxidation; current applications of these techniques and a discussion of the effects of change on O_2 evolution are provided.

5. •• Yachandra VK, Sauer K, Klein MP: **Manganese cluster in photosynthesis: where plants oxidize water to dioxygen.** *Chem Rev* 1996, **96**:2927-2950.
A detailed molecular structure of the $(Mn)_4$ cluster and of the likely association of the two non redox-active cofactors in water oxidation, Ca^{2+} and Cl^-, with the tetranuclear site has been derived from X-ray absorption studies; a model for water oxidation that invokes oxidation of bridging oxos is described.

6. • Rüttinger W, Dismukes GC: **Synthetic water-oxidation catalysts for artificial photosynthetic water oxidation.** *Chem Rev* 1997, **97**:1-24.
Model compound work to produce a water-oxidizing catalyst is attracting considerable attention and effort and this development is reviewed.

7. •• Tommos C, Babcock GT: **Oxygen production in nature: a light-driven metalloradical enzyme process.** *Accounts Chem Res* 1998, **31**:18-25.
The hydrogen atom abstraction model for water oxidation is summarized and a series of thermodynamic, kinetic, and structural tests are applied to it. Functional roles for Ca^{2+} and Cl^- in water oxidation are postulated, and the likely involvement of Jahn-Teller effects at the Mn ions in promoting these functions is considered.

8. Tommos C, Tang X-S, Warncke K, Hoganson CW, Styring S, McCracken J, Diner BA, Babcock GT: **Spin-density distribution, conformation, and hydrogen bonding of the redox-active tyrosine Y_Z in photosystem II from multiple electron magnetic-resonance spectroscopies: implication for photosynthetic oxygen evolution.** *J Am Chem Soc* 1995, **117**:10325-10335.

9. Hoganson CW, Lydakis-Simantiris N, Tang X-S, Tommos C, Warncke K, Babcock GT, Diner BA, McCracken J, Styring S: **A hydrogen-atom abstraction model for the function of Y_Z in photosynthetic oxygen evolution.** *Photosynth Res* 1995, **46**:177-184.

10. Gilchrist ML Jr, Ball JA, Randall DW, Britt RD: **Proximity of the manganese cluster of photosystem II to the redox-active tyrosine Y_Z.** *Proc Natl Acad Sci USA* 1995, **92**:9545-9549.

11. •• Tang X-S, Randall DW, Force DA, Diner BA, Britt RD: **Manganese-tyrosine interaction in the photosystem II oxygen-evolving complex.** *J Am Chem Soc* 1996, **118**:7638-7639.
The assignment of the split electron paramagnetic resonance signal in cofactor-depleted PSII as arising from the $S_2Y_Z^{\bullet}$ state is proven by isotope labeling at the tyrosine.

12. Debus RJ: **The manganese and calcium ions of photosynthetic oxygen evolution.** *Biochim Biophys Acta* 1992, **1102**:269-352.

13. Babcock GT: **The oxygen-evolving complex in photosystem II as a metallo-radical enzyme.** In *Photosynthesis: from Light to Biosphere*, vol II. Edited by Mathis P. Dordrecht: Kluwer Academic Publishers; 1995:209-215.

14. •• Hoganson CW, Babcock GT: **A metalloradical mechanism for the generation of oxygen from water in photosynthesis.** *Science* 1997, **277**:1953-1956.
The rate-limiting step in O_2 evolution is the reduction of the $Y_Z^{\bullet}$ species; a molecular mechanism for O-O bond formation that rationalizes this observation within the context of a concerted process involving $Y_Z^{\bullet}$ and substrate bond as Mn^{IV}=O and Mn^{IV}-OH is presented and analyzed. This mechanism has general applicability to a range of enzymatic reactions.

15. Force DA, Randall DW, Britt RD: **Proximity of acetate, manganese, and exchangeable deuterons to tyrosine $Y_Z^{\bullet}$ in acetate-inhibited photosystem II membranes: implications for the direct involvement of $Y_Z^{\bullet}$ in water-splitting.** *Biochemistry* 1997, **36**:12062-12070.

16. Riggs-Gelasco PJ, Mei R, Ghanotakis DF, Yocum CF, Penner-Hahn JE: **X-ray absorption spectroscopy of calcium-substituted derivatives of the oxygen-evolving complex of photosystem II.** *J Am Chem Soc* 1996, **118**:2400-2410.

17. Vass I, Styring S: **pH-dependent charge equilibria between tyrosine-D and the S states in photosystem II. Estimation of relative midpoint redox potentials.** *Biochemistry* 1991, **30**:830-839.

18. Mahoney LR, DaRooge MA: **The kinetic behavior and thermochemical properties of phenoxy radicals.** *J Am Chem Soc* 1975, **97**:4722-4731.

19. Foti M, Ingold KU, Lusztyk J: **The surprisingly high reactivity of phenoxy radicals.** *J Am Chem Soc* 1994, **116**:9440-9447.

20. Lind J, Shen X, Eriksen TE, Merényi G: **The one-electron reduction potential of 4-substituted phenoxy radicals in water.** *J Am Chem Soc* 1990, **112**:479-482.

21. •• Blomberg MRA, Siegbahn PEM, Styring S, Babcock GT, Åkermark B, Korall P: **A quantum chemical study of hydrogen abstraction from manganese-coordinated water by a tyrosyl radical: a model for water oxidation in photosystem II** *J Am Chem Soc* 1997, **119**:8285-8292.
High-level density functional theory methods are used to calculate bond dissociation energies for water, phenol, and manganese-ligated H_2O and OH^-; the accuracy of the computational approach to these critical parameters was later demonstrated by experiments.

22. Gardner KA, Mayer JM: **Understanding C-H bond oxidation: H• and H⁻ transfer in the oxidation of toluene by permanganate.** *Science* 1995, **269**:1849-1851.

23. Baldwin MJ, Pecoraro VL: **Energetics of proton-coupled electron transfer in high-valent $Mn_2(\mu\text{-}O)_2$ systems: models for water oxidation by the oxygen-evolving complex of photosystem II.** *J Am Chem Soc* 1996, **118**:11325-11326.

24. •• Caudle MT, Pecoraro VL: **Thermodynamic viability of hydrogen atom transfer from water coordinated to the oxygen-evolving complex of photosystem II.** *J Am Chem Soc* 1997, **119**:3415-3416.
Careful thermodynamic cycle analysis is applied to Mn-cluster-coordinated water to show that the bond dissociation energy of H_2O decreases by

~35 kcal/mol when complexed to the metal relative to its value in bulk solution.

25. Haumann M, Bögershausen O, Cherepanov D, Ahlbrink R, Junge W: **Photosynthetic oxygen evolution: H/D isotope effects and the coupling between electron and proton transfer during the redox reactions at the oxidizing side of photosystem II.** *Photosynth Res* 1997, **51**:193-208.

26. Karge M, Irrgang K-D, Renger G: **Analysis of the reaction coordinate of photosynthetic water oxidation by kinetic measurements of 355 nm absorption changes at different temperatures in photosystem II preparations suspended in either H_2O or D_2O.** *Biochemistry* 1997, **36**:8904-8913.

27. Lydakis-Simantiris N, Ghanotakis DF, Babcock GT: **Kinetic isotope effects on the reduction of the Y_Z radical in oxygen evolving and tris-washed photosystem II membranes by time-resolved EPR.** *Biochim Biophys Acta* 1997, **1322**:129-140.

28. Boussac A, Sétif P, Rutherford AW: **Inhibition of tyrosine Z photooxidation after formation of the S_3 state in Ca^{2+}-depleted and Cl^--depleted photosystem II.** *Biochemistry* 1992, **31**:1224-1234.

29. Razeghifard MR, Klughammer C, Pace RJ: **Electron paramagnetic resonance kinetic studies of the S states in spinach thylakoids.** *Biochemistry* 1997, **36**:86-92.

30. • Razeghifard MR, Pace RJ: **Electron paramagnetic resonance kinetic studies of the S states in spinach PSII membranes.** *Biochim Biophys Acta* 1997, **1322**:141-150.

The rates of the individual S-state advances, that is, $S_nY_Z^{\bullet} \rightarrow S_{n+1}Y_Z$, are shown to be sensitive functions of the methods used for sample preparation; the $S_3 \rightarrow S_4 \rightarrow S_0 + O_2$ reaction is demonstrated to have the greatest sensitivity. Taken together, these observations suggest atom-transfer processes rather than simple electron transfers as underlying the accumulation of oxidizing potential on the $(Mn)_4$ cluster.

31. Cha Y, Murray CJ, Klinman JP: **Hydrogen tunneling in enzyme reactions.** *Science* 1989, **243**:1325-1330.

32. Boussac A, Zimmermann J-L, Rutherford AW, Lavergne J: **Histidine oxidation in the oxygen-evolving photosystem-II enzyme.** *Nature* 1990, **347**:303-306.

33. Hallahan BJ, Nugent JHA, Warden JT, Evans MCW: **Investigation of the origin of the 'S_3' EPR signal from the oxygen-evolving complex of photosystem 2: the role of tyrosine Z.** *Biochemistry* 1992, **31**:4562-4573.

34. MacLachlan DJ, Nugent JHA, Warden JT, Evans MCW: **Investigation of the ammonium chloride and ammonium acetate inhibition of oxygen evolution by photosystem II.** *Biochim Biophys Acta* 1994, **1188**:325-334.

35. Khangulov S, Sivaraja M, Barynin VV, Dismukes GC: **The dimanganese(III,IV) oxidation state of catalase from *Thermus thermophilus:* electron nuclear double resonance analysis of water and protein ligands in the active site.** *Biochemistry* 1993, **32**:4912-4924.

36. Coffman RE, Buettner GR: **A limit function for long-range ferromagnetic and antiferromagnetic super exchange.** *J Phys Chem* 1979, **83**:2387-2392.

37. •• Noguchi T, Inoue Y, Tang S-X: **Structural coupling between the oxygen-evolving Mn cluster and a tyrosine residue in photosystem II as revealed by Fourier transform infrared spectroscopy.** *Biochemistry* 1997, **36**:14705-14711.

Distance estimates between $Y_Z^{\bullet}$ and $(Mn)_4$ in earlier work had been criticized, as they were not carried out with oxygen-evolving material; this paper provides the first experimental demonstration that a short separation between the radical and the metal cluster occurs for the native system as well.

38. • Åhrling KA, Peterson S, Styring S: **An oscillating manganese electron paramagnetic resonance signal from the S_0 state of the oxygen evolving complex in photosystem II.** *Biochemistry* 1997, **36**:13148-13152.

Until this work and that in [39•] no EPR signal had been detected from the S_0 state; this development will provide significant new insight into the structure and properties of the $(Mn)_4$ cluster in water oxidation.

39. • Messinger J, Robblee JH, Yu WO, Sauer K, Yachandra VK, Klein MP: **The S_0 state of the oxygen-evolving complex in photosystem II is paramagnetic: detection of an EPR multiline signal.** *J Am Chem Soc* 1997, **119**:11349-11350.

See annotation [38•].

40. Ferguson-Miller S, Babcock GT: **Heme/copper terminal oxidases.** *Chem Rev* 1996, **96**:2889-2907.

41. Lancaster CRD, Michel H, Honig B, Gunner MR: **Calculated coupling of electron and proton transfer in the photosynthetic reaction center of *Rhodopseudomonas viridis*.** *Biophys J* 1996, **70**:2469-2492.

42. Lavergne J, Junge W: **Proton release during the redox cycle of the water oxidase.** *Photosynth Res* 1993, **38**:279-296.

43. • Rappaport F, Lavergne J: **Charge recombination and proton transfer in manganese-depleted photosystem II.** *Biochemistry* 1997, **36**:15294-15302.

A careful comparison of proton release and chlorophyll bandshifts that accompany the oxidation and reduction of Y_Z which shows that the two processes are not necessarily correlated.

44. •• Ahlbrink R, Haumann M, Cherepanov D, Bögershausen O, Mulkidjanian A, Junge W: **Function of tyrosine Z in water oxidation by photosystem II: electrostatical promotor instead of hydrogen abstractor.** *Biochemistry* 1998, **37**:1131-1142.

A detailed and thoughtful criticism of the function of Y_Z as a hydrogen atom abstractor during water oxidation; proton release measurements, chlorophyll bandshifts and isotope effects are used in this assessment.

45. Babcock GT, Callahan PM: **Redox-linked hydrogen bond strength changes in cytochrome a: implications for the cytochrome oxidase proton pump.** *Biochemistry* 1983, **22**:2314-2319.

46. Mulkidjanian AY, Cherepanov DA, Haumann M, Junge W: **Photosystem II of green plants: topology of core pigments and redox cofactors as inferred from electrochromic difference spectra.** *Biochemistry* 1996, **35**:3093-3107.

47. Diner BA, Tang S-X, Zheng M, Dismukes GC, Force DA, Randall DW, Britt RD: **Environment and function of the redox active tyrosines of photosystem II.** In *Photosynthesis: from Light to Biosphere*, vol II. Edited by Mathis P. Dordrecht: Kluwer Academic Publishers; 1995:229-234.

48. • Zhang H, Razeghifard MR, Fischer G, Wydrzynski T: **A time-resolved FTIR difference study of the plastoquinone Q_A and redox-active tyrosine Y_Z interactions in photosystem II.** *Biochemistry* 1997, **36**:11762-11768.

The first use of time-resolved Fourier transform infrared spectroscopy to study water oxidation provides a clear assignment of vibrational modes that are linked to the oxidation and reduction of Y_Z; the coupling of this process to vibrational perturbation of a chlorophyll is proposed.